

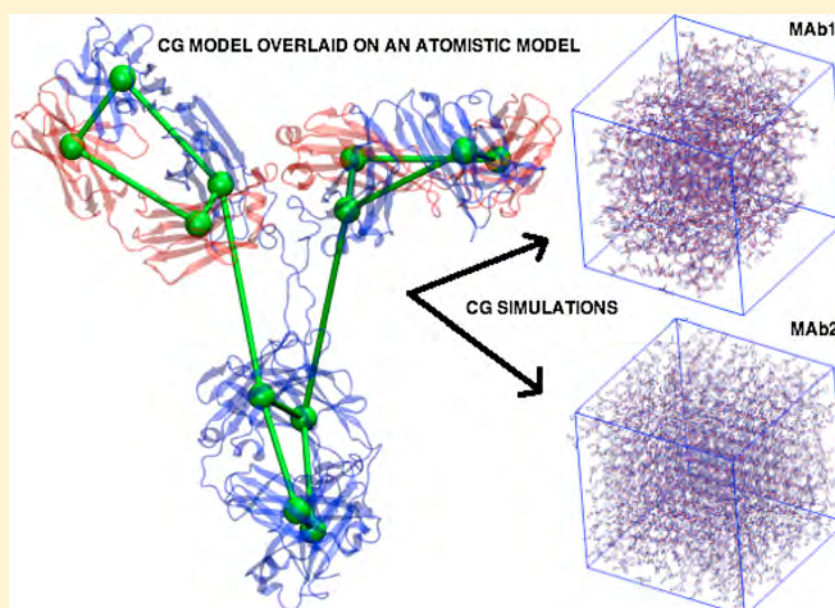
Coarse-Grained Modeling of the Self-Association of Therapeutic Monoclonal Antibodies

Anuj Chaudhri,[†] Isidro E. Zarraga,^{*,‡} Tim J. Kamerzell,[‡] J. Paul Brandt,[§] Thomas W. Patapoff,[§] Steven J. Shire,[‡] and Gregory A. Voth^{*,†}

[†]Department of Chemistry, James Franck Institute, Institute for Biophysical Dynamics and Computation Institute, University of Chicago, Chicago, Illinois 60637, United States

[‡]Late Stage Pharmaceutical Development and [§]Early Stage Pharmaceutical Development, Genentech Inc., 1 DNA Way, South San Francisco, California 94080, United States

S Supporting Information



ABSTRACT: Coarse-grained computational models of two therapeutic monoclonal antibodies are constructed to understand the effect of domain-level charge–charge electrostatics on the self-association phenomena at high protein concentrations. The coarse-grained representations of the individual antibodies are constructed using an elastic network normal-mode analysis. Two different models are constructed for each antibody for a compact Y-shaped and an extended Y-shaped configuration. The resulting simulations of these coarse-grained antibodies that interact through screened electrostatics are done at six different concentrations. It is observed that a particular monoclonal antibody (hereafter referred to as MAb1) forms three-dimensional heterogeneous structures with dense regions or clusters compared to a different monoclonal antibody (hereafter referred to as MAb2) that forms more homogeneous structures (no clusters). These structures, together with the potential mean force (PMF) and radial distribution functions (RDF) between pairs of coarse-grained regions on the MAbs, are qualitatively consistent with the experimental observation that MAb1 has a significantly higher viscosity compared to MAb2, especially at concentrations >50 mg/mL, even though the only difference between the MAbs lies with a few amino acids at the antigen-binding loops (CDRs). It is also observed that the structures in MAb1 are formed due to stronger Fab–Fab interactions in corroboration with experimental observations. Evidence is also shown that Fab–Fc interactions can be equally important in addition to Fab–Fab interactions. The coarse-grained representations are effective in picking up differences based on local charge distributions of domains and make predictions on the self-association characteristics of these protein solutions. This is the first computational study of its kind to show that there are differences in structures formed by two different monoclonal antibodies at high concentrations.

Received: February 4, 2012

Revised: June 9, 2012

Published: June 13, 2012

■ INTRODUCTION

Immunotherapy serves to improve the immune system to treat infectious diseases either actively through vaccines or passively through therapeutic monoclonal antibodies (MAbs).¹ Targeting diseases through monoclonal antibodies has achieved a lot of success with 29 U.S. Food and Drug Administration (FDA) approved MAbs in the market² and many more in the pipeline.³ These monoclonal antibodies require very high doses (>1 mg/kg) to be administered to a patient due to potency issues. The usual route of administration until now has been intravenous, but this leads to higher patient care costs and the need for skilled workers. On the other hand, subcutaneous delivery (SC) is a more convenient route of administration. However, this route poses an upper limit on the dosage volume that can be administered at a given time, typically <1.5 mL, and thus necessitates the development of formulations for SC administration at concentrations >100 mg/mL. High-concentration protein solutions pose formulation challenges such as high viscosity during manufacturing,^{4,5} protein stability issues leading to association and aggregation,^{6,7} and degradation of the drug.^{8,9} Protein aggregation not only can lead to processing and manufacturing issues, but also may cause undesired immunogenic responses in the body.¹⁰ Hence, understanding the issues of self-association and aggregation can lead to more stable therapeutic drugs that can be administered in a more risk-free manner with limited patient costs.

High-concentration protein formulation development will require an understanding of protein–protein interactions (PPI), especially when the average distance between the molecules is greatly diminished.¹¹ The solution behavior is also highly nonideal with the solution showing viscoelastic properties. Protein–protein interactions in general include hydrogen bonding, excluded volume, electrostatic, hydrophobic, and van der Waals dispersion forces. A number of experimental studies have been done to characterize the behavior of these high-concentration solutions and analyze the most important PPI that govern the behavior of concentrated antibody solutions. Liu et al.¹² studied the viscosity behavior of three monoclonal antibodies as a function of concentration, pH, and ionic strength. They found that one of the antibodies (MAB1, same as the one studied here) showed sharp viscosity changes with concentration. MAB1 at 125 mg/mL was found to be 60-fold more viscous than the solution without protein. The viscosity of MAB1 was also dependent on the shear rate at high concentrations, and its viscosity was shown to decrease with increasing ionic strength. The high viscosity of MAB1 was attributed to the reversible self-association behavior of these protein molecules in solution. On the basis of the decreasing viscosity with addition of salt, it was hypothesized that electrostatic charge–charge interactions were perhaps the most important PPI in solution, whereas for MAB2 (same as the one studied here), the nonideal behavior of the solution with concentration was mainly due to the excluded volume effect. In particular, MAB2, but not MAB1, viscosity data as a function of concentration could be accounted for by a modified version of the extended Mooney equation,¹² which only takes into account excluded volume effects. Kanai et al.¹³ performed a series of titration studies on the MAB1 solutions and concluded that the Fab–Fab interaction between MAbs was the key contributor to the formation of an organized multivalent network.

Additionally, Yadav et al.^{14,15} have done extensive experimental studies on different mAb solutions at different pH values, ionic strengths, and concentrations. To probe the interactions between the MAbs, they used dynamic light scattering to measure the mutual diffusion constant of moving particles using

an autocorrelation function to fit the time decay of scattering intensity. At low ionic strength of 15 mM, the MAB1 solutions show a positive interaction parameter at pH 4.0 and 9.0. Between pH values of 5.0 and 7.0, a negative interaction parameter is observed. The value is most negative at pH 6.0 indicating that the interactions are the most attractive at this pH value. The ultrasonic shear rheometry experiments were used to measure the solution storage modulus that exhibits a sharp increase above 80 mg/mL at pH 6.0. The storage modulus is shown to peak at pH of 6.0 at high concentrations, which is indicative of strong attractive interactions. On adding salt to the solutions, the solution modulus decreased, which indicates a decrease in the protein–protein interactions due to shielding. This signifies the importance of electrostatic interactions as opposed to hydrophobic interactions in forming strong networks owing to strong attractive forces between the protein molecules.

On comparing different MAbs, Yadav et al.¹⁵ found that the viscosity profiles for the IgG1MAbs cannot be explained solely on the basis of the electroviscous effects or the net-charge induced intermolecular repulsions. They also showed that the differences in viscosity behavior could not be attributed to the molecular size based on intrinsic viscosity analysis. They attributed the viscosity behavior to the nature of the intermolecular interactions, in particular, short-range attractive potentials between specific domains of the MAbs. They concluded that specific short-range electrostatic interactions arising from charge–dipole and dipole–dipole interactions could be causing an enhanced effect on the molecules, which leads to a self-associating network to form resulting in large viscosity changes. Hence, testing the hypothesis that electrostatics beyond the mAb net charge may play a vital role in differentiating between MAbs has to be done systematically. Computational models can help fill in this gap where experiments might be difficult to perform.¹⁶

Numerical simulations using molecular dynamics (MD)^{17,18} have come a long way from just being applied to small liquid systems. Enhanced computational power has given way to very large biomolecular systems having a million atoms being simulated with considerable increase in computational speed.¹⁹ However, issues still remain, as most of the processes that are interesting in nature span over multiple length and time scales, and often traditional MD cannot treat this disparity in time and length scales. For example, one mAb in a solvated environment requires running simulations for over 300 000 atoms. About 1000 of these MAbs would be well over 300 million atoms. Simulating this system using MD is intractable. Hence, alternative techniques need to be used to help understand processes at higher length and longer time scales. Coarse-grained (CG) and structurally reduced models of biosystems help bridge the long time and length scale gap and make biological processes more accessible.^{20–22} These CG methodologies have been applied to a large number of systems and have shed light on many fundamental processes (see a recent review²³ and the examples within).

In this paper, we investigate the role of charge–charge electrostatics at the domain level in self-association of two therapeutic monoclonal antibodies hereby referred to as MAB1 and MAB2. Experiments have pointed to electrostatics being important in forming networks and leading to differences in solution properties. To test this hypothesis, as a first approximation, a novel simulation methodology has been developed to understand the highly complex multiscale problem of self-association. Two reduced coarse-grained models (12 site and 26 site) of these antibodies have been developed, and coarse-grained molecular dynamics (CGMD) simulations were

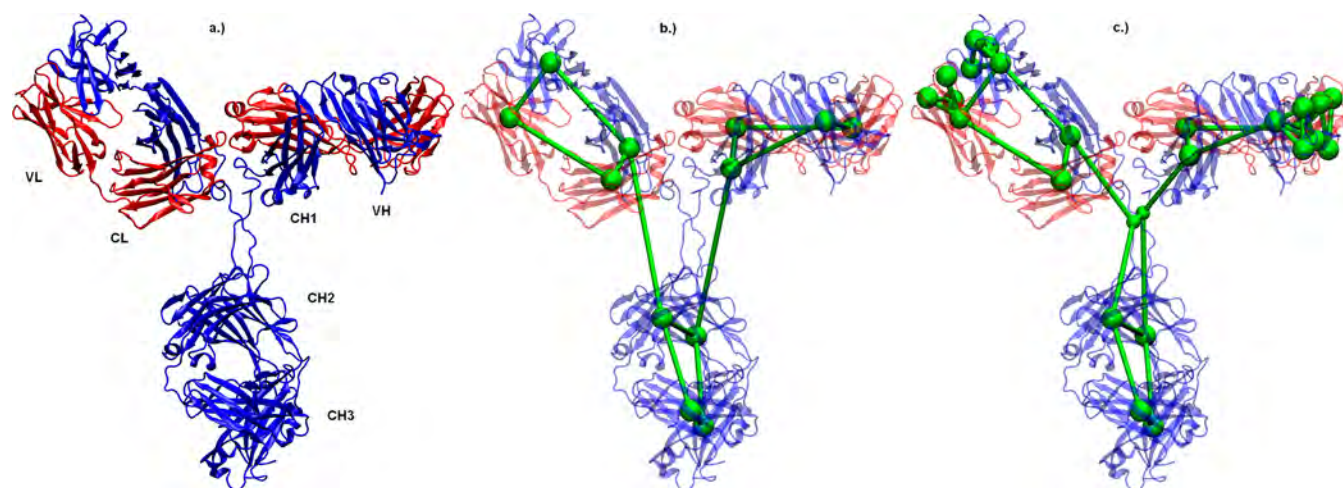


Figure 1. Monoclonal antibody structure and CG models. (a) Actual 3D structure of the IgG1 monoclonal antibody.²⁴ The antibody contains two identical heavy and light chains. The heavy chain contains four domains: VH, CH1, CH2, and CH3. The light chain contains two domains: VL and CL. (b) 12 site CG model overlaid on the 3D structure of the antibody. (c) 26 site CG model overlaid on the 3D structure of the antibody. The figures were rendered using VMD.⁴⁵

performed as a function of concentration. The systems were tested at a pH value of 6.0, since this is the recommended pH for storage where chemical degradations are minimized. To test the effect of 3D geometry (Fab–Fab angle) on the simulations, two different configurations of the antibody structure were tested—a Y-shaped model with a Fab–Fab angle of 36° and an extended Y-shaped model with a Fab–Fab angle of 130° . Additionally, simulations were also done on flexible CG models of the antibodies by incorporating the intramolecular interactions between different domains in the antibody. Specifically the hypothesis of enhanced Fab–Fab interactions for MAb1 is tested in these simulations. The following sections of this article are organized as follows. In methods, we explain the techniques developed and used to construct the reduced mAb model, utilizing a normal mode elastic network analysis of a proposed solution structure based on MD simulations.²⁴ The results section present the CGMD simulations performed on the CG models of the antibodies showing the effects of the coarse-grained resolution, geometry, and flexibility on the association process. The results are assessed further in the discussion section, where the differences in structures formed by the antibodies are clearly shown and corroborated with experimental data wherever possible.

METHODS

IgG1 monoclonal antibodies are very large Y-shaped four chain polypeptides.²⁵ Each subunit consists of two types of chains referred to as the light and heavy chains. The light and heavy chains are interfaced through disulfide bonds between cysteine amino acids on each chain. The heavy chains consist of four domains each, whereas the light chains consist of two domains each. Overall, the IgG1 antibody contains 12 domains as seen in Figure 1. In addition to the disulfide bonds, a carbohydrate chain also stabilizes the two heavy chains. The following notation that is consistent with all the other antibody structures²⁶ will be employed: heavy chains consist of constant domains denoted as CH1, CH2, and CH3 and a variable domain VH. Light chains consist of one constant domain CL and one variable domain VL. The CH2 and CH3 domains from the heavy chains together form the Fc (fragment crystallizes easily) region of the mAb. The VH, VL, and CH1 domains form the Fab (fragment antigen binding) region of the mAb. The VH and VL domains each contain three

antigen binding loops referred to as the CDR regions. The hinge region of the antibody lies between CH1 and CH2 domains of the heavy chain. The hinge regions of the two heavy chains are also linked via disulfide bridges between its cysteine residues.

The general approach to identify and construct CG representations requires the identification of CG site positions within each protein domain and the CG effective potential parameters. The strategies for the two tasks are discussed below. The mAb 3D structure framework was based on an MD model for MAb2 that is the most likely conformation in solution.²⁴ The MAb1 representation uses the same framework. It is important to note that it is extremely difficult to obtain experimentally the crystal structure of a full-length mAb due to poor crystallization or extreme flexibility of the hinge region (see ref 24 and references therein). In their study, Brandt et al.²⁴ pieced together a full structure of the IgG1 antibody from crystal structures of the fragments and equilibrated it in silico to a relaxed conformation. This relaxed structure was used to construct the representative CG models. Due to the unavailability of the full IgG1 crystal structure, it is also difficult to ascertain the correct Fab–Fab and Fab–Fc angles. Hence, in this study, two different CG configurations were used—a Y-shaped configuration with a Fab–Fab angle of 36° (from the relaxed MD configuration) and an extended Y-shaped configuration with a Fab–Fab angle of 130° (arbitrarily chosen to be an obtuse angle), hereafter referred to as compact and extended configurations, respectively. Both configurations use the same underlying residue framework.

Identification of Coarse-Grained Sites. Two kinds of mAb CG models were developed—one with 12 sites and another with 26 sites. The 12 site model was developed by performing an elastic network normal-mode analysis²⁷ that places the CG sites based on the long-wavelength dynamic motion of the protein domains. It is known that collective protein motions play an important role in their biological function.^{28,29} In this procedure, an elastic network model of the protein is used to calculate the low-frequency modes, which are then used to define the dynamically correlated domains and the CG representation. It was found that each domain of the antibody moved as a whole unit in the low frequency limit. Hence, the center of mass of each domain was chosen for the placement of the corresponding CG site. The sites were numbered from 1 to 12 as shown in Figure 2.

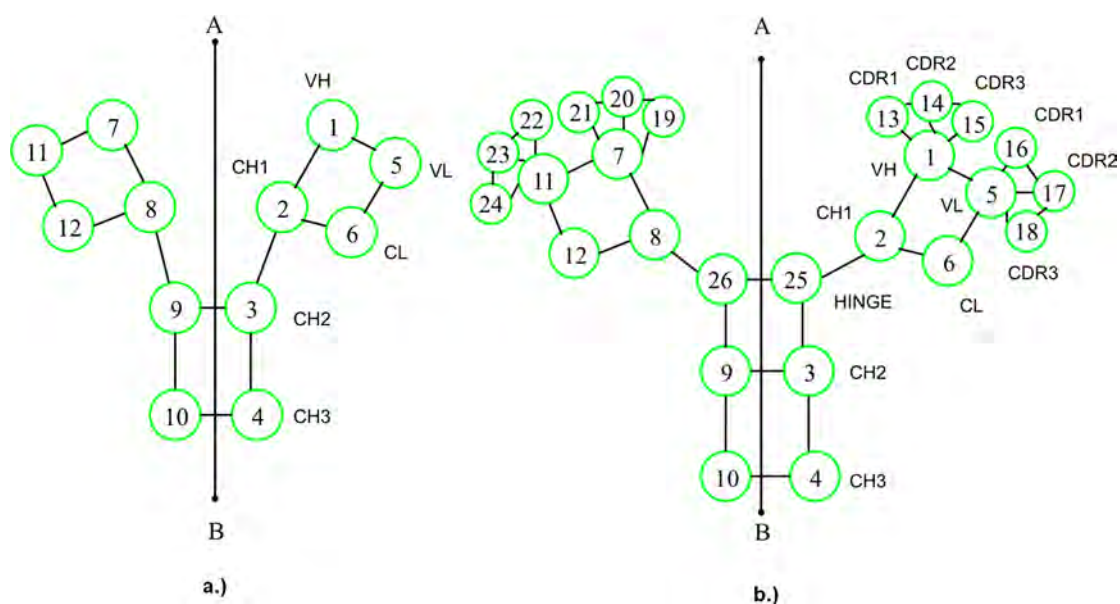


Figure 2. CG representations of the monoclonal antibody molecule. The schematic shows all the sites and site numbers used to identify the different regions of the mAb. The antibody is symmetric with respect to the heavy and light chains through the plane AB that divides the antibody in half. (a) 12 site lower-resolution model; (b) 26 site higher-resolution model.

It is important to note that the mAb is C_2 -symmetric (twofold symmetry) with respect to the heavy and light chains through the plane AB that divides the mAb as seen in Figure 2. Hence, sites 1 and 7, 2, and 8, and so forth, are identical with respect to the underlying residues they represent. However, the three-dimensional structure in Figure 1 show that the mAb is not symmetric geometrically about plane AB. The 26 site model uses the same structure as the 12 site model except that extra sites are added to the CDR regions and a CG site is added to the center of mass of the hinge region as shown in Figure 2. The total mass and charge of each CG site was calculated by summing up the masses and partial charges respectively of the underlying residues that the site represents. The partial charges were based on the CHARMM force field.³⁰ According to the Henderson–Hasselbalch equation, histidine is about 50% protonated at pH 6.0. Hence, it was assumed that each histidine residue contributes a partial charge of +0.5 units at pH 6.0. The masses and charges for each domain at pH 6 are shown in Table 1. In the 12 site model, the mass and charge of the hinge region are divided equally between sites 2 and 3. In the 26 site model, sites 25 and 26 represent the underlying hinge residues. It is important to note that the charge distribution of the MAb is reduced to the coarse-grained bead level to specifically test the effect of domain-level charge–charge electrostatics on self-association.

Coarse-Grained Force Field. The coarse-grained variables represent collective degrees of freedom of multiple atoms in a protein domain. Hence, the interactions between the CG sites have to be chosen to represent large-scale protein motion in an averaged, effective manner. The local fluctuations of individual atoms are averaged over and effective interactions are considered. A typical, classical, effective potential can be written as a sum of intraprotein and interprotein interactions as follows:

$$U_{\text{total}} = U_{\text{intra}} + U_{\text{inter}} \quad (1)$$

The bond, angle, and dihedral potential functions constitute the intraprotein interactions, whereas the electrostatic and dispersion forces constitute the interprotein interactions. The bonds, angles, and dihedrals that connect different CG domains were defined

Table 1. Masses and Charges Used in All the CG Simulations^a

site number	(a) 12 Site Model			
	mass (amu)		charge at pH 6	
	MAB1	MAB2	MAB1	MAB2
1, 7	13506	13536	+3.5	+3.5
2, 8	10854.5	11027.5	+2.75	+3.75
3, 9	12552.5	12552.5	+3.25	+3.25
4, 10	12047	12047	−0.5	−0.5
5, 11	12389	12277	−1.5	+4.5
6, 12	11398	11162	−2	−2
site number	(b) 26 Site Model			
	mass (amu)		charge at pH 6	
	MAB1	MAB2	MAB1	MAB2
1, 7	8936	8882	+1	+2
2, 8	9997	10170	+3	+4
3, 9	11695	11695	+3.5	+3.5
4, 10	12047	12047	−0.5	−0.5
5, 11	8997	9455	+3	+4
6, 12	11398	11162	−2	−2
13, 19	1159	1132	0	+0.5
14, 20	1756	2016	0	+2
15, 21	1655	1506	+2.5	−1
16, 22	1688	1113	−2	0
17, 23	721	756	−1	0
18, 24	983	953	−1.5	+0.5
25, 26	1715	1715	−0.5	−0.5

^aThe masses and charges were calculated as a cumulative sum of all the underlying residues in each CG site. The charges at pH 6 assume HIS to be 50% protonated and have a net positive charge of +0.5.

based on the structure obtained from the MD simulations. More information on the definition of the bonds, angles, and dihedrals can be found in the Supporting Information. The effect of the topology of the mAb and electrostatics on self-association is by itself a very important problem to study in protein solutions.³¹ The effect of the internal degrees of freedom on the self-association characteristics is

tested separately by including the intramolecular interactions to the CG models already developed.

Interprotein Interactions. The interprotein interactions can be divided into electrostatic and dispersion forces. The screened electrostatics and van der Waals interactions are assumed to be independent of each other and additive as in the Derjaguin-Landau-Verwey-Overbeek theory of colloidal particle interactions.³² The electrostatic interactions were modeled by the Coulomb potential with Debye-Hückel screened electrostatics³² having an exponential Yukawa term.

$$U_{\text{coulomb}} = \frac{q_i q_j}{4\pi\epsilon_r r} \exp(-\kappa r) \quad (2)$$

Here, q_i and q_j represent the net charges on the CG sites, ϵ_r is the effective dielectric constant, and κ is the Debye screening parameter. The effective dielectric constant refers to the screening effect of the apparent interaction energy compared to the vacuum interaction. Calculating the effective dielectric constant of protein solutions has been the subject of many investigations.³³ In the absence of a distance-dependent screening term, the effective dielectric constant in the presence of explicit water may vary from a value of 2 inside the protein to 4 on the outer surface of the protein.³⁴ However, no consensus has been found on the best way to calculate the effective dielectric constant within and between two protein molecules especially for implicit solvent models.^{35,36} When the interaction is screened as in eq 2, the proper value of the effective dielectric constant is less clear. In this study, we assume a screened implicit solvent model with an effective dielectric constant of 1. A more detailed study on the exact value of the effective dielectric constant will be the subject of future investigations. A value of 2.5 nm is used for the Debye screening length, which is the inverse of the Debye screening parameter κ . The value was picked based on experimental investigations using 15 mM salt solutions.^{14,15} The dispersion and repulsive forces due to excluded volume were modeled using a Lennard-Jones potential with a force smoothing function.

$$U_{\text{LJ}} = 4\epsilon_{ij} \left[\left(\frac{\sigma_{ij}}{r} \right)^{12} - \left(\frac{\sigma_{ij}}{r} \right)^6 \right] \quad r < r_{\text{in}} \quad (3)$$

$$F = C_1 + C_2(r - r_{\text{in}}) + C_3(r - r_{\text{in}})^2 + C_4(r - r_{\text{in}})^3 \quad r_{\text{in}} < r < r_c \quad (4)$$

where ϵ_{ij} is the well depth for the ij th pair of CG sites and σ_{ij} is the radius at which LJ potential is exactly zero. It separates the hard repulsive region of the potential from the attractive well. In eq 4, r_{in} is the inner cutoff radius and r_c is the outer cutoff radius for pairs of CG site interactions. The polynomial coefficients C_1 , C_2 , C_3 , and C_4 are computed on the fly to smoothly vary the force from the inner cutoff to the outer cutoff.³⁷ The σ_{ij} value for the LJ potential (shown in Table 2) was chosen based on the average size of each domain. It is the distance at which the hard-sphere repulsion between domains becomes important. The well depth is chosen to be much weaker than the strength of the hydrogen bond. Further investigations into the variation of the LJ parameters will be the subject of future investigations.

Intraprotein Interactions. The bond, angle, and dihedral interactions for the MAbs were defined based on harmonic approximations to the interaction strength.

$$U_{\text{bond}} = k_{\text{bond}}(r - r_0)^2 \quad (5)$$

$$U_{\text{angle}} = k_{\text{angle}}(\theta - \theta_0)^2 + k_{\text{UB}}(r - r_{\text{UB}})^2 \quad (6)$$

Table 2. Pair Interaction Potential Parameters for the CG Models Used in the Simulations

simulation parameter	value
ϵ_r	1.0
κ	0.04 (Å) ⁻¹
ϵ_{ij}	1.0 kcal/mol
σ_{ij}	20.0 Å
r_{in}	100 Å
r_c	200 Å
timestep	1 ps for rigid MAbs 20 ns for flexible MAbs
Langevin bath damping parameter	5 ps
Langevin bath temperature	300 K
total number of time steps	5 000 000 for rigid MAbs 30 000 000 for flexible MAbs

$$U_{\text{dihedral}} = k_{\text{dihedral}}[1 + \cos(\varphi - d)] \quad (7)$$

where k_{bond} , k_{angle} , k_{UB} , and k_{dihedral} are the spring constants for the bond, angle, Urey-Bradley (UB), and dihedral terms. The UB term is an additional interaction term that is specified between the first and third particle in the angle. The equilibrium bond, angle, UB, and dihedral terms are defined by r_0 , θ_0 , r_{UB} , and d in eqs 5–7. The spring constants and equilibrium values for the intramolecular interactions were computed using 8 different MD trajectories of 60 ns each that were generated independently.²⁴ More details regarding the calculation of these values can be found in the Supporting Information.

Langevin dynamics simulations were performed to capture the effect of the solvent friction. Using the CG sites and the force field described in the above sections, equilibrium CGMD simulations of the 12 and 26 site models were performed using the LAMMPS package.³⁷ The simulation parameters for the models are listed in Table 2. Initially, 1000 mAb molecules were arranged in a cubic lattice and the system was allowed to run for 5 μ s until it reaches equilibrium. This was confirmed when the rmsd of the system from the initial configuration reached a plateau. The final configuration from the equilibrated trajectory was then heated to an elevated temperature to ensure that all the MAbs have random orientations and are not stuck in a metastable state. The final configuration from this second run is then used as the initial condition for all the simulations. Annealing techniques such as slow cooling from a high temperature was not tried here, which might lead to different final equilibrated structures, but it is expected that the overall behavior and clustering differences between the MAbs will still be the same. Periodic boundary conditions were applied in all three directions. The CGMD simulations were performed under constant (particle number, volume, temperature) NVT conditions using a Langevin thermostat with the temperature set to 300 K. At each time step, a stochastic force with a random orientation and magnitude consistent with thermal motion at 300 K was applied to each CG site. The relaxation constant associated with the Langevin dynamics was fixed at 5 ps based on the viscosity of water at 300 K. The CG simulations for the rigid antibodies were run for 5 million iterations using a time step of 1 ps. This corresponds to 5 μ s of CGMD simulation time with the first 1 million iterations chosen as the equilibration time. The remaining 4 million iterations were chosen to calculate all of the properties and time-averaged data. For the flexible antibodies, the simulations were run for 30 million iterations at a time step of 20 ns, as flexibility introduces additional degrees of freedom that reduce the time step.

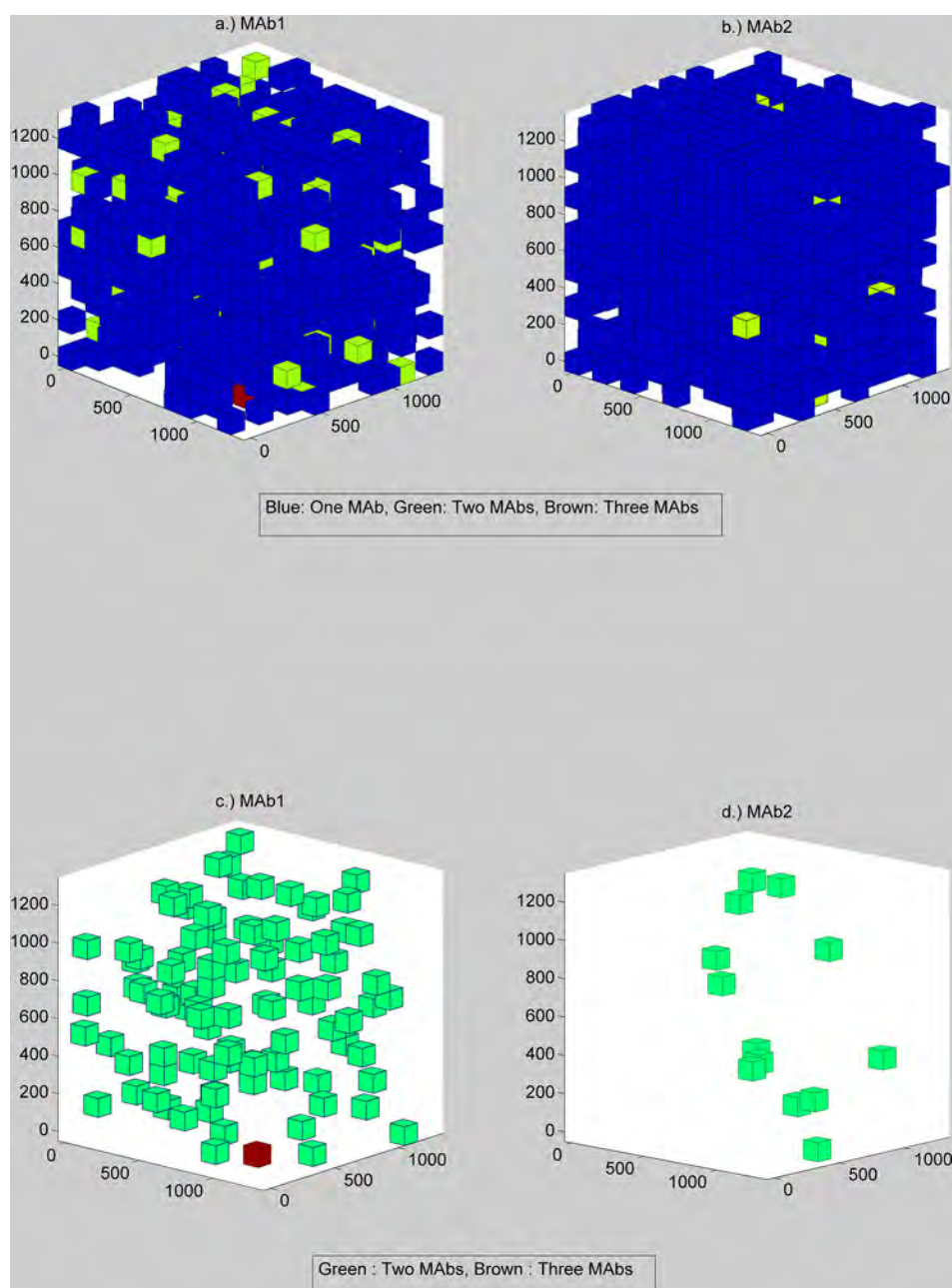


Figure 3. Distribution of equilibrated structures of the compact Y-shaped 12 site rigid MAb1 and MAb2 model systems at pH 6, 120 mg/mL. The distribution is shown for (a,c) MAb1 and (b,d) MAb2 systems. The distribution was calculated by dividing the domain into cubic boxes of size 100 Å each and counting the number of MAbs in each cube. The cubes are colored according to the number of MAbs within them. The cubes with one mAb center are colored blue, the ones with two MAbs are colored green, and those with three MAbs are colored brown.

RESULTS

The CG models described above were used to study the effect of the charge distribution on the self-association of the two Genentech antibodies under different conditions. Langevin dynamics simulations were performed on these MAbs to obtain equilibrium structures at the end of the simulations. The results from the simulation studies are discussed below.

Twelve Site Rigid Model Using the Compact Configuration. Simulations were performed at different concentrations starting from 20 to 120 mg/mL at pH 6. The equilibrium structures obtained at the end of the simulations showed self-associated structures being formed in the MAb1 system as compared to MAb2. Figure 3 shows the distribution of the

equilibrated structures at 120 mg/mL for both MAb1 and MAb2 systems at pH 6. The distribution shown in the figure was calculated by dividing the domain into cubic boxes of side 100 Å. Within each cube, the number of mAb centers (of masses) is counted, and the cubes are colored according to the number of mAb centers inside them. Figure 3a,b shows the distribution of the cubes in MAb1 and MAb2 systems at 120 mg/mL, respectively. Figure 3c,d is the same as Figure 3a,b showing cubes containing more than one mAb center. It is interesting to note that MAb1 has a higher distribution of cubes that have two or more mAb centers compared to MAb2 as seen in Figure 3c,d. The distribution of MAb1 centers in Figure 3c is scattered all across the domain compared to MAb2 where only a few scattered cubes can be seen (Figure 3d).

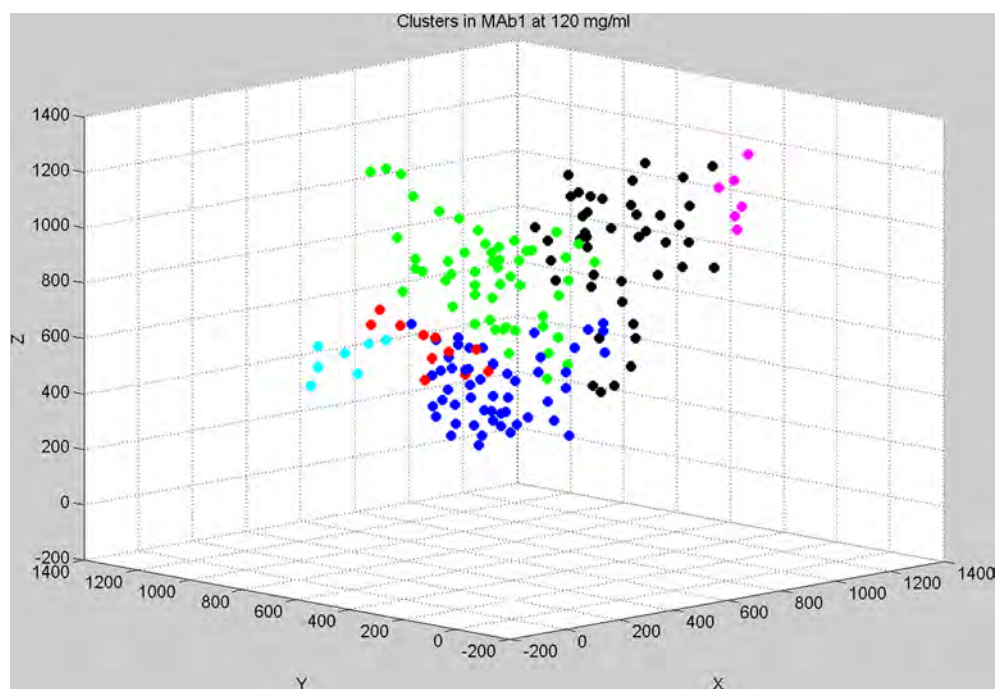


Figure 4. Cluster formation in the equilibrated structure of the compact Y-shaped 12 site rigid MAb1 model at pH 6 and 120 mg/mL. The clustering was calculated using the density-based clustering algorithm DBSCAN. The centers of masses of the MAbs were used for this calculation. Six different clusters were identified in the domain and have been colored accordingly. All the centers that belong to a cluster have the same color.

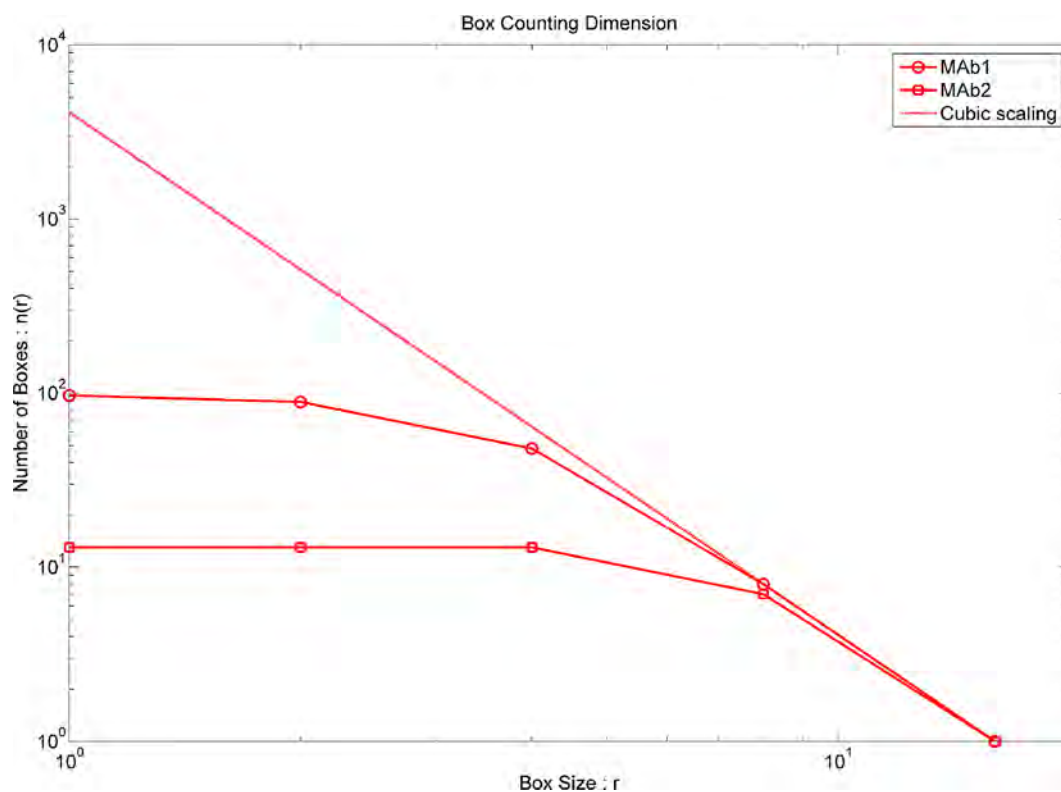


Figure 5. Box counting dimensions of both MAb1 and MAb2 systems using equilibrated structures of the compact Y-shaped 12 site rigid model at pH 6 and 120 mg/mL. The distribution of MAbs shown in Figure 3c,d were used as starting configurations for the calculations. The box size r shown in the figure is scaled so that $r = 1$ corresponds to $r = 100$ Å. $n(r)$ counts the number of boxes required to cover the entire domain for a given box size. The figure shows that in MAb1 systems the distribution of mAb centers is such that more boxes would be required to cover the entire domain compared to MAb2 systems.

To show further evidence that MAb1 forms dense structures at higher concentrations, clustering calculations were done on the

equilibrated mAb structures at 120 mg/mL using DBSCAN, a density-based clustering algorithm.^{38,39} The clusters were

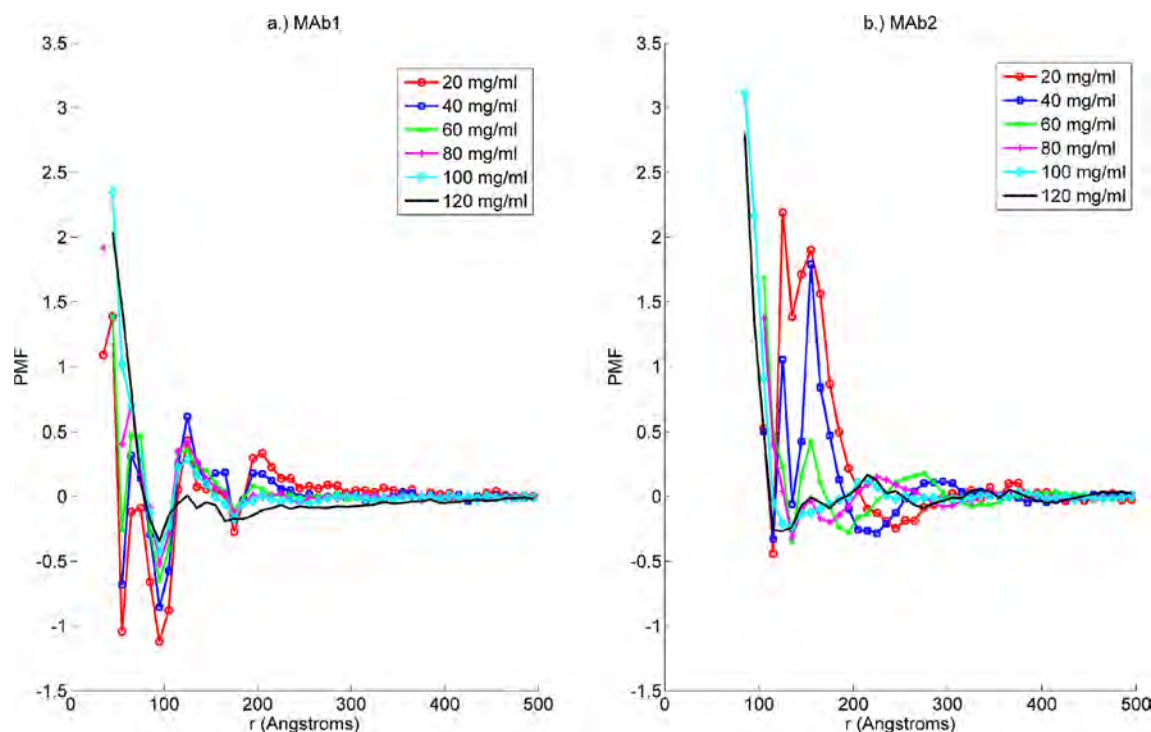


Figure 6. Potential of mean force (PMF) plots (in kcal/mol) as a function of concentration for the compact Y-shaped 12 site rigid model at pH 6. The PMF is calculated using eq 5 from the equilibrium center of mass (COM) distribution of the MABs. Panel (a) shows the PMF for MAB1 for concentrations 20–120 mg/mL. MAB1 systems show more short-range attractions compared to MAB2 systems in panel (b) that show more short-range repulsions.

defined based on the criteria that a minimum of 4 mAb centers are found within a neighborhood radius of 100 Å. The algorithm gave evidence of six clusters of varying sizes spread across the domain in MAB1 at 120 mg/mL. The clusters are shown in Figure 4 and the mAb centers colored according to the cluster they belong to. All other mAb centers that do not belong to any cluster have been removed to allow better visualization of the clustering. The same algorithm returned no clusters in MAB2 pointing to a more homogeneous distribution of MABs. The differences in equilibrium structure formation between MAB1 and MAB2 at 120 mg/mL can be studied further by calculating the box-counting dimension or the Minkowski-Bouligand dimension of Figure 3c,d.^{40,41} The plot showing the number of boxes required to cover all the cubes in Figure 3c,d as a function of the box dimension is shown in Figure 5. The slope of the curves is the box-counting dimension for the particular system. It can be seen that a large number of boxes are required to cover the entire space in MAB1 compared to MAB2 thereby pointing to the differences in equilibrium structure at 120 mg/mL. The distribution of cubes containing two or more mAb centers is dense in MAB1 at 120 mg/mL compared to MAB2, which can clearly be seen from Figure 5.

To understand the effect of higher concentrations on the association characteristics of the MABs, the radial distribution function (RDF) was calculated using the equilibrium center of mass (COM) distribution of the MABs. The RDF was then used to define a potential of mean force (PMF) in kcal/mol using the usual equation

$$\text{PMF} = -k_B T \ln[g(r)] \quad (8)$$

The PMF for MAB1 and MAB2 at pH 6 is plotted in Figure 6 as a function of concentration. It can be clearly seen that the two mAb systems behave very differently at both lower and higher

concentrations. The MAB1 systems have more short-range attraction as evidenced by the sharp minima in the PMF shown in Figure 6. The figure shows two sharp minima separated by a barrier of 1 kcal/mol. The barrier height decreases with concentration and completely disappears at 100 mg/mL. For the MAB2 systems, the short-range attractions are less dominant. The potential minimum is not as deep when compared to MAB1 systems. In contrast, MAB2 systems show more short-range repulsions than strong attractions at low concentrations. As the concentration increases, the repulsive barrier found between 100 and 200 Å decreases in height and disappears at 100 mg/mL. MAB1 systems also show the potential minimum at distances less than 100 Å compared to MAB2. To understand which interactions between the MABs are the most prominent, radial distribution functions (RDFs) for site–site interactions were calculated. The CG site numbers are given in Figure 2. The site–site interactions can be broken down into Fab–Fab, Fc–Fc, and Fab–Fc. The Fab–Fab interactions between the MABs were calculated for site numbers 1–1, 7–7, 5–5, 11–11, 1–5, 7–11, 1–11, 1–7, 5–11, and 5–7. The Fab–Fc interactions between the MABs were calculated for site numbers 4–1, 4–7, 4–5, 4–11, 10–1, 10–7, 10–5, and 10–11. The RDFs for the Fab–Fab interactions are plotted in Figures 7 and 8 and Fab–Fc interactions in Figure 9 respectively.

The RDF in Figure 7 shows considerable short-range structure for MAB1 systems as compared to MAB2 systems. The maximum in the RDF for MAB1 systems occurs at less than 50 Å compared to MAB2 at 100–120 Å. Also, the RDF for MAB1 is more erratic and contains a number of smaller peaks as compared to MAB2 systems, which is much smoother in comparison. The presence of multiple peaks and rougher landscape for MAB1 is indicative of local ordering similar to solid-like structures, and provides a measure of the correlation length of the cluster or network. In

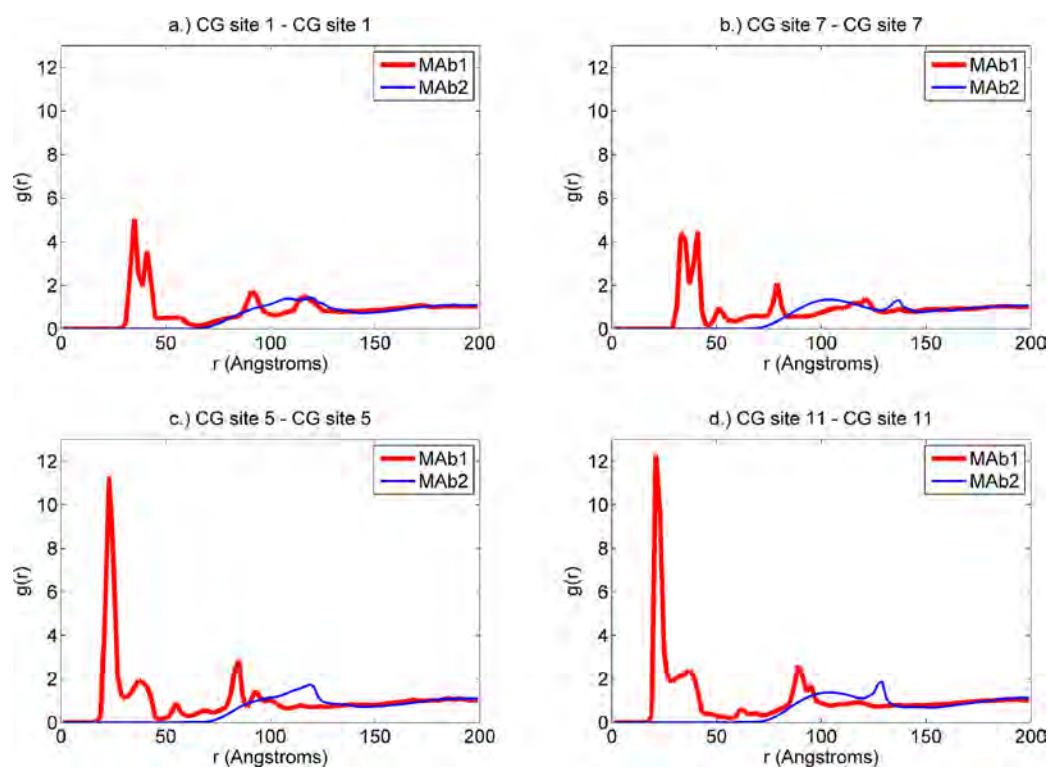


Figure 7. Radial distribution function (RDF) plots for the compact Y-shaped 12 site rigid model at pH 6 and 120 mg/mL. The figure shows the Fab–Fab interactions in MAb1 (thick line) and MAb2 (thin line) for (a) CG site 1–CG site 1, (b) CG site 7–CG site 7, (c) CG site 5–CG site 5, and (d) CG site 11–CG site 11. The site numbering is shown in Figure 2a. The figures show that MAb1 has significant short-range structure compared to MAb2. Also, the MAb1 RDF is more solid-like compared to MAb2.

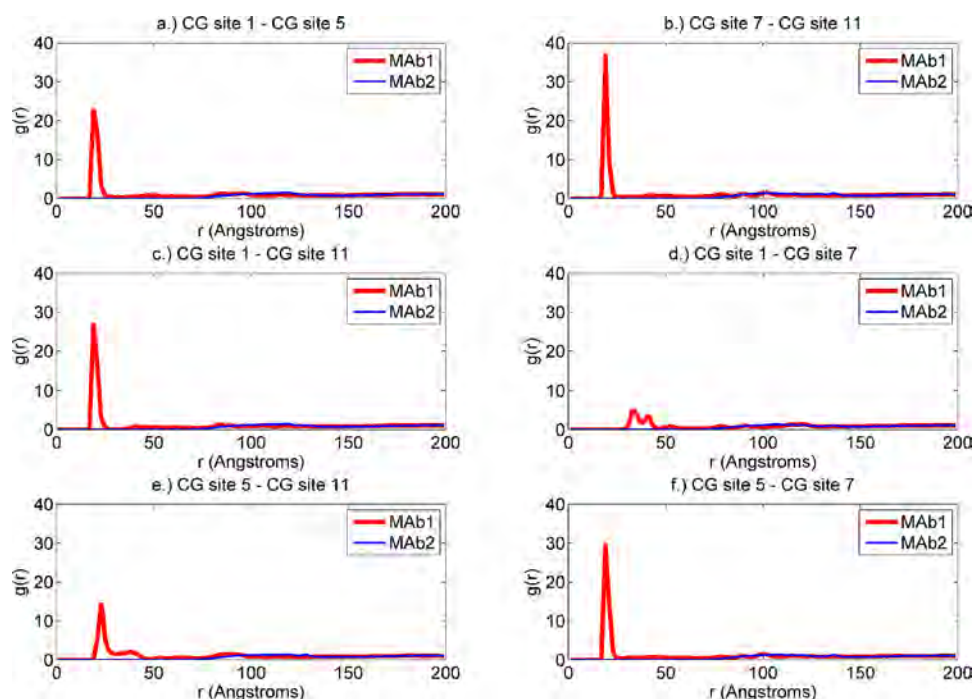


Figure 8. Radial distribution function (RDF) plots for the compact Y-shaped 12 site rigid model at pH 6 and 120 mg/mL. The figure shows the Fab–Fab interactions in MAb1 (thick line) and MAb2 (thin line) for (a) CG site 1–CG site 5, (b) CG site 7–CG site 11, (c) CG site 1–CG site 11, (d) CG site 1–CG site 7, (e) CG site 5–CG site 11, and (f) CG site 5–CG site 7. The site numbering is shown in Figure 2a. The figures show MAb1 systems to have more short-range structure compared to MAb2 especially in panels (c), (e), and (f).

contrast, the smoother, more “fluid-like” RDF for MAb2 is indicative of a more randomized and homogeneous structure. This is apparent in the equilibrated structures in Figure 3 that

show dense structuring for MAb1 and more homogeneous structuring for MAb2 solutions. Figure 8 shows the time-averaged RDF for sites 1–5, 7–11, 1–11, 1–7, 5–11, and 5–7. It

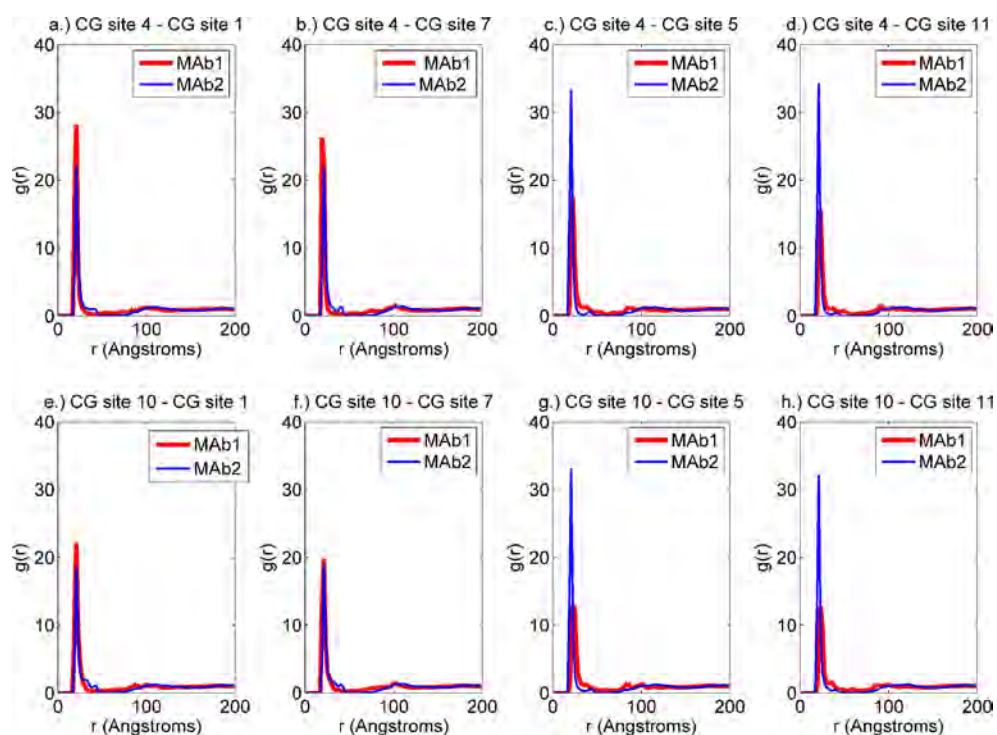


Figure 9. Radial distribution function (RDF) plots for the compact Y-shaped 12 site rigid model at pH 6 and 120 mg/mL. The figure shows the Fab–Fc interactions for (a) CG site 4–CG site 1, (b) CG site 4–CG site 7, (c) CG site 4–CG site 5, (d) CG site 4–CG site 11, (e) CG site 10–CG site 1, (f) CG site 10–CG site 7, (g) CG site 10–CG site 5, and (h) CG site 10–CG site 11. The site numbering is shown in Figure 2 a. The Fab–Fc interactions are stronger in the MAb2 systems compared to MAb1 thus resulting in the more homogeneous structures.

Table 3. Quantitative Assessment of the Fab–Fab, Fab–Fc, and Fc–Fc Interactions in the CG Simulations from the Site–Site Radial Distribution Functions

mAb	area under the curve: Fab–Fab interactions		area under the curve: Fab–Fc interactions		area under the curve: Fc–Fc interactions		ratio of Fab–Fab to all interactions		ratio of Fab–Fc to all interactions		ratio of Fc–Fc to all interactions	
	1	2	1	2	1	2	1	2	1	2	1	2
12 site, rigid, compact Y	2052.8	1210.3	1852.3	1832.6	567.6	586.2	0.46	0.33	0.41	0.51	0.13	0.16
12 site, flexible, compact Y	2466.8	1139.1	2164.3	2181.9	593.2	409.6	0.47	0.31	0.41	0.58	0.11	0.11
12 site, rigid, extended Y	2029.7	1252.7	1686.2	2062.5	424.6	375.3	0.49	0.34	0.41	0.56	0.1	0.1
26 site, rigid, compact Y	2082.3	1202.5	2077.8	1803.2	485.4	385.5	0.45	0.36	0.45	0.53	0.11	0.11

is interesting to note that these interactions are much stronger compared to those in Figure 7 evidenced by the scale of the graph in Figure 8. The 5–7, 7–11, and 1–11 are the strongest interactions for MAb1 molecules due to the strong positive and negative charges on these sites. Also, the 3D geometric structure of the MAbs gives rise to a preferential interaction of these sites compared to other ones. The Fab–Fc interactions are plotted in Figure 9. The 4–5, 4–11, 10–5, and 10–11 interactions are the strongest in the case of MAb2. The preference for sites 5 and 11 is comparable to 1 and 7 due to the charge distribution on these sites and the 3D orientation of the mAb. Figure 7 suggests a stronger Fab–Fc interaction for MAb2 systems compared to Fab–Fab interactions.

To compare the strength of the different interactions in both MAb1 and MAb2, the area under the RDF plots was calculated for both MAb1 and MAb2 at 120 mg/mL using numerical quadrature. The data for all the models is reported in Table 3. It is interesting to note that both Fab–Fab and Fab–Fc interactions are equally dominant in MAb1 compared to MAb2 where Fab–Fc interactions are most dominant. The Fc–Fc interactions are the least dominant among the three. The importance of Fab–Fab

interactions in MAb1 at high concentrations has also been confirmed experimentally.¹³ The CG models corroborate this observation and additionally point to the importance of Fab–Fc interactions in both MAb1 and MAb2. The absence of dominating Fab–Fab interactions in MAb2 gives rise to a more homogeneous equilibrium structure compared to MAb1 where dense clusters are found spread across the domain.

Comparison of Simulations between the 12 and 26 Site Rigid Models Using the Compact Configuration.

Simulations were repeated for all the concentrations at pH 6 using the 26 site higher-resolution CG model. This was mainly done to understand the effect of adding extra sites to the CDR regions of the antibody on the self-association phenomena. The RDFs for the extra site–site interactions were calculated as before. The strength of the interactions was assessed by calculating the area under the RDF curves for both MAb1 and MAb2 and reported in Table 3. From Table 3, it is seen that both the Fab–Fab and Fab–Fc interactions are dominant for MAb1 whereas the Fab–Fc interactions are most dominant for MAb2. This is similar to what was found for the compact Y-shaped 12 site rigid model.

Additional comparisons of the lower and higher resolution models at a pH value of 6 were carried out by calculating the PMF for the COM distribution of the MABs using eq 8 (not shown here for brevity). The PMF for two mAb models at 120 mg/mL concentration shows clearly that the 12 and 26 site models show very similar behavior for both MAB1 and MAB2 at pH 6. The simulations indicate that the MAB1 systems form solid-like long-range structure at pH 6. However, MAB2 systems do not show the same long-range structure as MAB1 systems do. Overall, the equilibrated structures at pH 6, using the higher resolution 26 site models, compare very well with the structures observed with the lower resolution 12 site model. It is thus reassuring that the overall behavior shown by the 26 site model is very similar to that previously observed using the 12 site model.

Comparison of Simulations Using the Rigid Compact Vs the Rigid Extended Configurations. In order to assess the sensitivity of the model to the overall geometry of the molecule, simulations were done using the compact vs extended configurations. The intersite RDFs for the Fab–Fab and Fab–Fc interactions for the extended configuration at pH 6 are used to calculate the area under the curves (Table 3). The Fab–Fab and Fab–Fc interactions are still the dominant interactions for MAB1 and Fab–Fc interactions for MAB2. Overall, the extended Fab–Fab configuration model shows very similar behavior to the compact Fab–Fab configuration model.

Effect of Intramolecular Interactions on Equilibrium Simulations of the 12 Site Compact Model. To assess the effect of flexibility on the self-association process, simulations were done on the 12 site compact Y model by incorporating intramolecular interactions between the CG sites. More information on the values of the spring constants and equilibrium internal coordinates can be found in the Supporting Information. The intersite RDFs for the Fab–Fab and Fab–Fc interactions show that MAB1 still shows the dominant Fab–Fab and Fab–Fc interactions compared to MAB2 (RDFs not shown for brevity). Overall, flexibility introduces additional degrees of freedom for the antibody, but the behavior at high concentrations is very similar to that of the rigid model as seen in Table 3. For the Fab–Fc interactions, MAB2 shows the dominant interaction compared to MAB1. The overall behavior still remains very similar to that of the rigid models that were described previously.

DISCUSSION

The CG model simulations presented here suggest that domain-level charge–charge electrostatics can help differentiate among the equilibrium structures formed by the two antibodies studied here. Both the high-resolution and low-resolution CG models of the MABs were able to predict the differences in self-association characteristics between the two MABs. Experiments have shown that the two Genentech MABs show very different viscosity behavior with an increase in concentration. The MAB1 molecules show sharp viscosity changes as a function of increasing concentration, whereas the MAB2 systems show slower changes in viscosity with increase in concentration.¹² According to the CG simulations, these differences can be attributed to the kind of self-associating structures that are formed with an increase in concentration. Even though equilibrium structures by themselves are not enough to predict rheological behavior of these solutions, some inferences can be made based on them. The PMF plots in Figure 6 suggest that MAB1 systems interact via effective short-range interactions when compared to MAB2 solutions. The closely packed regions in the equilibrium structure of MAB1 at 120 mg/mL extend the correlation of the network to

larger distances. The formation of dense clusters in MAB1 at 120 mg/mL compared to none in MAB2 suggest that there could be a correlation between the ordering observed using CG models and the high viscosity observed experimentally. The MAB2 network appears more homogeneous at the various concentrations studied compared to MAB1's dense network. It is conceivable that this lesser tendency to cluster and the larger surface–surface distance (as indicated by the potential of mean force plots) allow the MAB2s to more easily slide past each other under shear flow, which translates to a lower viscosity.

At very high concentrations, e.g., 120 mg/mL, MAB2 appears to form homogeneous structures via Fab–Fc interactions. The PMF plots suggests that, even at these high concentrations, these homogeneous MAB2 structures may require less energy (or shear) to break loose compared the MAB1's dense structure. Since viscosity is typically measured under flow conditions, for a more accurate description of how the mAb network resists deformation or disruption under shear, nonequilibrium shear flow computations have to be performed as a function of concentration and will be the subject of future studies. In addition, a more complex model may be needed to describe behavior at very high concentrations (e.g., 100 mg/mL). Factors such as near-field hydrodynamic, hydrogen-bonding network,⁴² and specific ion binding effects⁴³ could have a significant contribution when the protein surfaces are very close to each other. The major difference between the MAB1 and MAB2 CG models in the present work lies in the net charge on the Fab domains, and this difference is enough for the two MABs to show very different self-association characteristics. The results therefore predict that effective domain-level electrostatic interactions can play a dominant role in the self-association of antibodies.

The simulation studies presented here point to the usefulness of CG models in predicting the important interactions between MABs at high concentrations. For example, the association in MAB1 is seen to be caused by enhanced Fab–Fab and Fab–Fc interactions, whereas the association in MAB2 is dominated by Fab–Fc interactions. The 3D geometry of the antibody makes it difficult for the antibodies to arrange themselves in a definite pattern. Hence, MAB1 systems tend to form clusters rather than a definite pattern. On the other hand, the more prevalent Fab–Fc association in MAB2 systems happens between the Fab arm on one antibody with the Fc tail of another one in its vicinity. The Fab arms carry a large net positive charge that causes strong electrostatic repulsions among them. However, the Fc tail is negatively charged and this leads to a favorable Fab–Fc interaction. This strong Fab–Fc interaction causes MAB2 systems to form homogeneous structures spread out over the domain.

The CG simulations further suggest that the higher resolution models developed here do not offer much more than the lower resolution models. The reason for this is that the long-range structures that MAB1 and MAB2 form are based on the net charge on the domains. Breaking the VH and VL domains into 4 CG sites (3 for CDR + 1 COM) does not do much in terms of changing the net electrostatic force between the MABs. It does, however, have an effect on the overall combination of the electrostatic and dispersion forces by shifting the potential energy minimum to a higher value. This causes the Fab arms to feel the effect of each other at a larger distance when compared to the lower resolution model. However, finer resolution models based on further refining the Fc domains have not been tested in this study and could perhaps shed more light on the Fab–Fc interactions. These models will be the subject of future

investigations. It is interesting to note that the extended Y-configuration shows very similar behavior to the compact Y-configuration. This further confirms the accuracy of the effective interactions. The wider Fab–Fab configuration suggests a Fab–Fab mediated structure formation for MAb1 systems in corroboration with the regular configuration and experiments. The MAb2 systems show structure formation via Fab–Fc interactions, which is similar to that predicted by the regular Y model. The effect of flexibility on the simulation results is to make the interactions between the two Fab arms and the Fc region more symmetric. The additional degrees of freedom offer more configuration space for the MAbs to move around and choose the best conformation possible. These simulations suggest that Fab–Fab and Fab–Fc interactions are still the dominating effect in MAb1 at high concentrations compared to MAb2 where Fab–Fc are most dominant. The results further confirm the idea that domain-level charge–charge electrostatics could help explain why MAb1 forms self-associated structures compared to MAb2.

The above simulation results predict that CG representations of the antibodies are indeed helpful in predicting the characteristic differences between the two MAbs. They have also been helpful in picking out the relative importance of the Fab–Fab and Fab–Fc interactions in MAb1 systems compared to the Fab–Fc interactions in MAb2 systems. This indicates that domain-level charge–charge electrostatics does play a vital role in the self-association of these antibodies. Other possibilities that include the tendency of IgG1s to bind to anions, which can have an impact on the surface charge distribution on the molecule,⁴³ have been neglected in the present model. It is also important to note that the results corroborate the experimental findings qualitatively and a more quantitative comparison with experimental results will be helpful to refine the CG models. For example, cryo-TEM and other high-resolution techniques such as light and neutron scattering can provide information about the mAb network geometry and scale. In fact, recent work on light scattering⁴⁴ estimates an apparent molecular weight as a function of concentration. The effective hard-sphere mixture model analysis shows that MAb1 self-associates to form oligomers with stoichiometry of 4–6 with an affinity that declines with increase in ionic strength. Some indication of this oligomer formation can be seen in Figure 3 c,d, where cubes with two or more mAb centers that are adjacent to each other are found all over the domain. This offers further confirmation on the usefulness of CG models in differentiating between MAbs that have varying properties. Determination of the structure factor, translation, and rotational diffusion at high concentrations using neutron scattering could provide another opportunity to compare and refine the CG simulations. It is clear currently that using these CG models to pick out relative differences between MAbs can be qualitatively very effective. However, the actual structures that are formed by the MAbs should be supplemented by more experimental investigations. The present work suggests that the models developed here can also be used to study the effect of changing the net charge on a domain of the antibody. Changing the net charge on the Fab domains should affect the self-association characteristics of these engineered antibodies. Performing CG simulations on mutants of the present antibodies could help ascertain differences between them easily. The CG models can thus be used as probes to check the effect of changing the net charge on the domains and to draw conclusions based on equilibrium structure formation.

CONCLUSIONS

This study examined the role that domain-level charge–charge electrostatics play in the self-association of two engineered therapeutic monoclonal antibodies, MAb1 and MAb2. Reduced coarse-grained models of the antibody were developed in the process using an elastic network normal-mode analysis. The results suggest that the MAb1 systems tend to form dense clusters compared to homogeneous structures for MAb2 systems. The self-association happens via Fab–Fab and Fab–Fc interactions in MAb1 and Fab–Fc interactions in MAb2. The dense structures might be responsible for the higher-viscosity trends found in experiments of high concentration MAb1 solutions. The homogeneous structures might be responsible for the slow variation of viscosity with concentration for MAb2 solutions. The results also suggest that charge–charge electrostatics plays a vital role in determining the equilibrium structures formed by the different MAbs due to differences in net charge of the domains. At the current resolution and approximation, the present model captures appreciable differences in network arrangements between MAb1 and MAb2 due to specific sequence differences in the CDR regions, and is consistent with certain experimental observations.

ASSOCIATED CONTENT

Supporting Information

Additional information as described. This material is available free of charge via the Internet at <http://pubs.acs.org>.

AUTHOR INFORMATION

Corresponding Author

*E-mail: zarraga.isidro@gene.com (I. Z.); gavoth@uchicago.edu (G. V.).

Notes

The authors declare no competing financial interest.

ACKNOWLEDGMENTS

This research was supported in part (A.C. and G.A.V.) by a National Science Foundation Grant Opportunity for Academic Liaison with Industry (GOALI) supplement (to grants CHE-0628257, CHE-1047323) and in part by the National Science Foundation through the Center for Multiscale Theory and Simulation (grant CHE-1136709). The computational resources for this work have been provided by a grant of supercomputing time provided by the U.S. Department of Defense (DoD) via project numbers AFPRD13233C3 V and AFPRD13233022. The computations were performed in part on Einstein (Cray XT5) at Navy DoD Supercomputing Resource Center (DSRC) and Jade (Cray XT4) at U.S. Army Engineer Research and Development Center (ERDC) DSRC.

REFERENCES

- (1) Waldmann, T. A. *Nat. Med.* **2003**, *9*, 269–277.
- (2) Aggarwal, S. *Nat. Biotechnol.* **2009**, *27*, 987–993.
- (3) Chan, A. C.; Carter, P. J. *Nat. Rev. Immunol.* **2010**, *10*, 301–316.
- (4) Shire, S. J.; Shahrokh, Z.; Liu, J. J. *Pharm. Sci.* **2004**, *93*, 1390–1402.
- (5) Shire, S. J. *Curr. Opin. Biotechnol.* **2009**, *20*, 708–714.
- (6) Cromwell, M. E.; Hilario, E.; Jacobson, F. *AAPS J.* **2006**, *8*, E572–579.
- (7) Shire, S. J.; Cromwell, M.; Liu, J. *AAPS J.* **2006**, *8*, E729–730.
- (8) Frokjaer, S.; Otzen, D. E. *Nat. Rev. Drug Discovery* **2005**, *4*, 298–306.
- (9) Daugherty, A. L.; Mrsny, R. J. *Adv. Drug Delivery Rev.* **2006**, *58*, 686–706.

- (10) Rosenberg, A. S. *AAPS J.* **2006**, *8*, E501–507.
- (11) Saluja, A.; Kalonia, D. S. *Int. J. Pharm.* **2008**, *358*, 1–15.
- (12) Liu, J.; Nguyen, M. D. H.; Andya, J. D.; Shire, S. J. *J. Pharm. Sci.* **2005**, *94*, 1928–1940.
- (13) Kanai, S.; Liu, J.; Patapoff, T. W.; Shire, S. J. *J. Pharm. Sci.* **2008**, *97*, 4219–4227.
- (14) Yadav, S.; Liu, J.; Shire, S. J.; Kalonia, D. S. *J. Pharm. Sci.* **2010**, *99*, 1152–1168.
- (15) Yadav, S.; Shire, S. J.; Kalonia, D. S. *J. Pharm. Sci.* **2010**, *99*, 4812–4829.
- (16) Laue, T.; Demeler, B. *Nat. Chem. Biol.* **2011**, *7*, 331–334.
- (17) Allen, M. P.; Tildesley, D. J. *Computer simulation of liquids*; Clarendon Press: Oxford, 1987.
- (18) Haile, J. M. *Molecular dynamics simulation: elementary methods*; Wiley: New York, 1992.
- (19) Stone, J. E.; Hardy, D. J.; Ufimtsev, I. S.; Schulten, K. *J. Mol. Graph. Model.* **2010**, *29*, 116–125.
- (20) Ayton, G. S.; Noid, W. G.; Voth, G. A. *Curr. Opin. Struct. Biol.* **2007**, *17*, 192–198.
- (21) Tozzini, V. *Acc. Chem. Res.* **2010**, *43*, 220–230.
- (22) Krishna, V.; Ayton, G. S.; Voth, G. A. *Biophys. J.* **2010**, *98*, 18–26.
- (23) Voth, G. A. *Coarse-graining of condensed phase and biomolecular systems*; CRC Press: Boca Raton, 2009.
- (24) Brandt, J. P.; Patapoff, T. W.; Aragon, S. R. *Biophys. J.* **2010**, *99*, 905–913.
- (25) Wang, W.; Singh, S.; Zeng, D. L.; King, K.; Nema, S. *J. Pharm. Sci.* **2007**, *96*, 1–26.
- (26) Brändén, C.-I.; Tooze, J. *Introduction to protein structure*, 2nd ed.; Garland Publishers: New York, 2009.
- (27) Zhang, Z.; Pfaendtner, J.; Grafmuller, A.; Voth, G. A. *Biophys. J.* **2009**, *97*, 2327–2337.
- (28) Kitao, A.; Go, N. *Curr. Opin. Struct. Biol.* **1999**, *9*, 164–169.
- (29) Berendsen, H. J.; Hayward, S. *Curr. Opin. Struct. Biol.* **2000**, *10*, 165–169.
- (30) Mackerell, A. D., Jr.; Feig, M.; Brooks, C. L., 3rd. *J. Comput. Chem.* **2004**, *25*, 1400–1415.
- (31) Levy, Y.; Onuchic, J. N. *Acc. Chem. Res.* **2006**, *39*, 135–142.
- (32) Larson, R. G. *The structure and rheology of complex fluids*; Oxford University Press: New York, 1999.
- (33) Matthew, J. B. *Annu. Rev. Biophys. Biophys. Chem.* **1985**, *14*, 387–417.
- (34) Simonson, T. *Rep. Prog. Phys.* **2003**, *66*, 737–787.
- (35) Sharp, K. A.; Honig, B. *Annu. Rev. Biophys. Biophys. Chem.* **1990**, *19*, 301–332.
- (36) Schutz, C. N.; Warshel, A. *Proteins* **2001**, *44*, 400–417.
- (37) Plimpton, S. J. *J. Comp. Phys.* **1995**, *117*, 1–19.
- (38) Ester, M.; Kriegel, H.; Sander, J.; Xu, X. *Proceedings of the Second International Conference on Knowledge Discovery and Data Mining (KDD-96)*; Portland, OR, 1996.
- (39) Daszykowski, M.; Walczak, B.; Massart, D. L. *Chemom. Intell. Lab. Syst.* **2001**, *56*, 83–92.
- (40) Schroeder, M. *Fractals, Chaos, Power Laws: Minutes from an Infinite Paradise*; W. H. Freeman: San Francisco, 1992.
- (41) Mandelbrot, B. B. *The fractal geometry of nature*; W. H. Freeman: San Francisco, 1982.
- (42) Kamerzell, T. J.; Kanai, S.; Liu, J.; Shire, S. J.; Wang, Y. J. *J. Phys. Chem. B* **2009**, *113*, 6109–6118.
- (43) Gokarn, Y. R.; Fesinmeyer, R. M.; Saluja, A.; Razinkov, V.; Chase, S. F.; Laue, T. M.; Brems, D. N. *Protein Sci.* **2011**, *20*, 580–587.
- (44) Scherer, T. M.; Liu, J.; Shire, S. J.; Minton, A. I. *J. Phys. Chem. B* **2010**, *114*, 12948–12957.
- (45) Humphrey, W.; Dalke, A.; Schulten, K. *J. Mol. Graph.* **1996**, *14*, 33–38.